Engineering Science and Technology, an International Journal 21 (2018) 215–228

HOSTED BY

Contents lists available at ScienceDirect

Engineering Science and Technology, an International Journal

journal homepage: www.elsevier.com/locate/jestch

Full Length Article

Chemically reactive and naturally convective high speed MHD fluid flow through an oscillatory vertical porous plate with heat and radiation absorption effect

S.M. Arifuzzaman [a], M.S. Khan [b,*], M.F.U. Mehedi [c], B.M.J. Rana [a], S.F. Ahmmed [a]

[a] Mathematics Discipline, Khulna University, Khulna 9208, Bangladesh
[b] Discipline of Chemical Engineering, University of Newcastle, Callaghan, NSW 2308, Australia
[c] Department of Thermal Science and Energy Engineering, University of Science and Technology of China, Anhui 230026, China

ARTICLE INFO

Article history:
Received 8 December 2016
Revised 31 October 2017
Accepted 5 March 2018
Available online 9 March 2018

Keywords:
MHD
Oscillating porous plate
Radiation absorption
High order chemical reaction
EFDM

ABSTRACT

This paper concerns with the modelling of an unsteady natural convective and higher order chemically reactive magnetohydrodynamics (MHD) fluid flow with the effect of heat and radiation absorption. The flow is generated through a vertical oscillating porous plate. Boundary layer approximations is carried out to establish a flow model which represents the time dependent momentum, energy and diffusion balance equations. Before being solved numerically, the governing partial differential equations (PDEs) were transformed into a set of nonlinear ordinary differential equation (ODEs) by using non-similar technique. A very efficient numerical approach solves the obtained nonlinear coupled ODEs so called Explicit Finite Difference Method (EFDM). An algorithm is implemented in Compaq Visual Fortran 6.6a as a solving tool. In addition, the stability and convergence analysis (SCA) is examined and shown explicitly. The advantages of SCA is its optimizes the accuracy of system parameters such as Prandtl number (P_r) and Schmidt number (S_c).The velocity, temperature and concentration fields in the boundary layer region are studied in detail and the outcomes are shown in graphically with the influence of various pertinent parameters such as Grashof number (G_r), modified Grashof number (G_r), magnetic parameter (M), Darcy number (D_a),Prandtl number (P_r), Schmidt number (S_c), radiation (R), heat sink (Q),radiation absorption (Q_1), Eckert number (E_c), Dufour number (D_u),Soret number (S_r), Schmidt number (S_c), reaction index (P) and chemical reaction (K_r). Furthermore, the effect of skin friction coefficient (C_f), Nusselt number (N_u) and Sherwood number (S_h) are also examined graphically.

1. Introduction

During the recent years, Magnetohydrodynamic (MHD) natural convection heat and mass transfer flow [1–10] is of significant attention in geophysics, engineering and industrial technology due to its wide range technical fields. This study finds numerous applications in industrial manufacturing processes such as the aerodynamic extrusion of plastic sheets, liquid metal fluids, biological transportation, oil reservoirs, geothermal systems, high-temperature plasmas, energy storage units, heat insulation and metal and polymer extrusion and micro MHD pumps etc. MHD flow through porous media is a major area of research for its wide range applications such as thermal energy storage devices, ground water systems, electronic cooling, boilers and nuclear process systems etc. Researchers are also interested in expanding their investigation on infinite vertical insulated porous plate [11], inclined porous plate [12], vertical porous plate [13–16], semi-infinite vertical porous plate [17] and vertical moving porous plate [18] etc.

In many chemical engineering and hydrometallurgical practices, it is required to investigate the influence of chemical reaction on heat and mass transfer flow because of the growing need for chemical reactions. This study is further plays outstanding role industries such as chemical industry, power and cooling industry for the applications of evaporation, flow in a desert cooler, energy transfer in a cooling tower, drying etc. Devi et al. [19] investigated chemical reaction effects on heat and mass transfer MHD boundary layer laminar type flow over a wedge considering suction/injection. Kandasamy et al. [20] studied chemical reactive MHD flow through a stretching surface with the effect of thermal stratification and heat source. The study of MHD temperature dependent

* Corresponding author.
E-mail address: md.s.khan@newcastle.edu.au (M.S. Khan).
Peer review under responsibility of Karabuk University.

https://doi.org/10.1016/j.jestch.2018.03.004
2215-0986/

Nomenclature

$B_\circ$	magnetic component
C_f	skin-friction
C_p	specific heat at constant pressure
D_a	Darcy number
D_m	coefficient of mass diffusivity
D_u	Dufour number
E_c	Eckert number
G_r	Grashof number
G_c	modified Grashof number
$K^/$	permeability of the porous medium
Kr	chemical reaction parameter
ke	mean absorption coefficient
N_u	local Nusselt number
P_r	Prandtl number
qr	unidirectional radiative heat flux
$Q1^*$	radiation absorption
$Q_\circ$	heat absorption quantity
S_c	Schmidt number
S_h	Sherwood number
S_r	Soret number
$U_\circ$	uniform velocity
u, v	velocity components
x, y	Cartesian co-ordinates

Greek symbols

σ	thermal conductivity
ρ	density of the fluid
μ	dynamic viscosities
ν	kinematic viscosity
β	thermal expansion co-efficient
β^*	concentration expansion co-efficient
κ	thermal conductivity
σs	Stefan-Boltzmann constant

viscosity and thermal diffusive flow with Hall and ion-slip currents with the influence of chemical reaction was carried out by Elgazery [21].The analysis of a first-order chemical reaction on MHD thermosolutal Marangoni convection flow was examined by Zhang and Zheng [22]. This field of study is still getting a lot of attention in recent years [23–31] for controlling the hydrodynamics behaviour of the fluid flow.

The fluid flow rising from the field of temperature and material difference is further applied in biochemical engineering, chemical engineering, geothermal reservoirs, aeronautics and astrophysics. The effect of presence of radiation absorption on the fluid flow is very significant from the scientific point of view. An example is arisen of this application in the planetary atmosphere where there is radiation absorption from nearby stars. Further industrial applications can be encompassed such as oil reservoirs, heat insulation, catalytic reactors, reactor safety, geothermal systems etc. Ibrahim et al. [32] reported the effect of radiation absorption on transient MHD free convection flow. Rubio Hernández [33] analysed a Network numerical analysis on unsteady MHD fluid flow through a porous medium with the influence of radiation absorption. Satya Narayana [34] investigated radiation absorption effects on MHD micropolar fluid flow in a rotating system. A study of free convective boundary layer flow with an aligned magnetic field in presence of radiation absorption was carried out by Reddy et al. [35]. The study of motion of fluids of magnetic field and thermal radiation effect on heat and mass transfer of air flow near a moving infinite plate with a constant heat sink has been studied by Arifuzzaman et al. [36] with Perturbation technique. The combined action of bouncy forces due to both thermal and mass diffusion in the presence of thermal radiation and chemical reaction are observed in nuclear reactor safety, solar collectors and combustion technique. Momentum boundary layer and thermal boundary layer presentation with the streamlines and isotherms has been studied by Rana et al. [37] in effect of radiation on unsteady MHD free convective flow past an exponentially accelerated inclined plate. A few more recent studies [38–41] can also be found where the radiation absorption parameter has a significant importance.

In many engineering applications including strength of radioactive materials, reactor safety analysis, spent nuclear fuel, fire and combustion, metal waste etc., it is very important to understand the effects of heat generation. This parameter is significant in numerous physical difficulties dealing with chemically reactive process and drives several phenomena (temperature distribution, particle deposition rate etc.) involve natural convection. The heat generation effects, MHD, heat and mass transfer flow has been studied by several researchers [42–47]. Recently, Reddy et al. [48] reported heat generation/absorption effects on MHD convective fluid flow (Al_2O_3–water and TiO_2–water nanofluids) past a stretching sheet in porous media. Srinivasa and Eswara[49] investigated the effect of heat generation on transverse magnetic-convective flow of an incompressible and electrically conducting fluid near an isothermal truncated cone. More recently, an analytical study MHD three-dimensional Oldroyd-B nanofluid flow with the effect of presence of heat generation/absorption is carried out by Hayat et al. [50]. Venkateswarlu and Satya Narayana [52] studied heat transfer flow of a nanofluid in a rotating system with the effect of radiation absorption and chemical reaction. Babu et al. [53] investigated the influence of radiation absorption on MHD transient free convection flow of a micropolar fluid through a porous medium of variable permeability over a vertical moving porous flat plate.

To the best of the author's knowledge, the study of transient MHD natural convective and chemically reactive high-speed fluid flow through an oscillatory vertical porous plate in presence of heat and radiation absorption has remained unexplored. Therefore, this phenomenon is addressed in this study. The results have been reported so far for MHD single-phase flow whilst hydrodynamic studies on high speed flow are reported only rarely. Application for high speed MHD are specially use in flow in the blanket (porous medium) of a nuclear fusion reactor, liquid metal MHD different phase flow power-generating etc. In the present investigation, the basic equation was derived, analysing the utmost MHD effects on flow momentum and energy transfer. For this reason, MHD term was also imposed in the thermal boundary layer equation. Theoretical solution for the effect of magnetic field on small convection-generating conditions was encompassed. The specific aims of this article are listed below:

To study the problem of unsteady chemically reactive fluid flow through a semi-infinite vertical porous plate with influence of thermal radiation, thermal and mass diffusion and radiation absorption, following steps have been carried out:

a) To solve the governing flow model including time dependent momentum, energy and diffusion balance equations numerically using well-known explicit finite difference method (EFDM).
b) Explicitly analyses the stability and convergence analysis (SCA) for optimizing the numerical value of flow parameters

as well as the high accuracy of the numerical investigation (EFDM).

c) To investigate the flow field distribution such as velocity, temperature and concentration across the boundary layer. Further investigation on system parameters effect of skin friction coefficient, Nusselt number and Sherwood number.

d) In addition, evaluate the momentum boundary layer and thermal boundary layer thickness with streamlines and isotherms.

2. Mathematical model of flow

Unsteady natural convective heat and mass transfer fluid flow along a semi-infinite vertical porous plate has been studied. In Fig. 1, y-axis is designed as normal to the vertical porous plate and the theoretical fluid flow analysis is considered in presence of uniform magnetic field, chemical reaction and thermal radiation. The flow is in the x-direction which is taken along the plate in the upward direction and y-axis is normal to it. For t > 0, the plate velocity, $U(t)$, oscillates with a frequency,γ, where the velocity on the wall can be expressed as $u = U_0 \cos(\gamma t)$. More precisely, the plate commences oscillation at y = 0 according to $u = U_0 \cos(\gamma t)$. Where, U_0 (constant) is the amplitude of the motion.

Initially, it is considered that the plate as well as the fluid particle is at rest at the same temperature $T(=T_\infty)$ and the same concentration level $C(=C_\infty)$ at all points. Where, C_∞ and T_∞ are fluid concentration and temperature species of uniform flow respectively. It is also assumed that a magnetic field $B_y = B_0$ of uniform strength is applied normal to the flow region. The physical configuration and co-ordinate system of the problem is presented in the following Fig. 1.

Continuity Equation:

$$\frac{\partial u}{\partial x}+\frac{\partial v}{\partial y}=0 \tag{1}$$

Momentum Equation:

$$\frac{\partial u}{\partial t}+u\frac{\partial u}{\partial x}+v\frac{\partial u}{\partial y}=\upsilon\frac{\partial^2 u}{\partial y^2}+g\beta(T-T_\infty)+g\beta^*(C-C_\infty)-\frac{\sigma' B_0^2 u}{\rho}-\frac{\upsilon}{K\prime}u \tag{2}$$

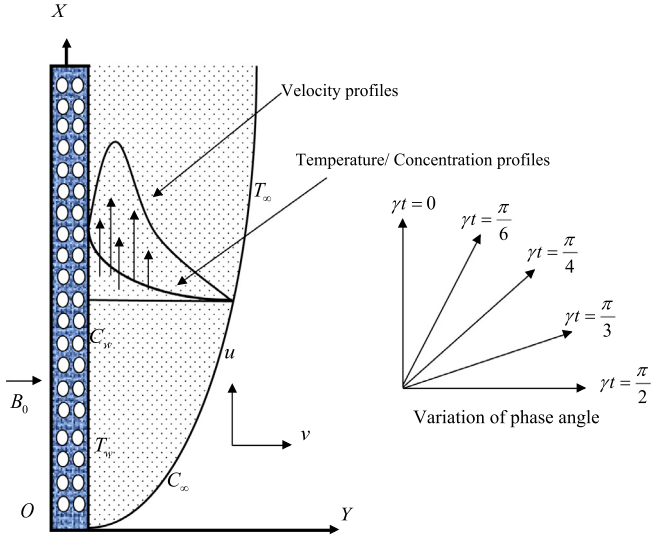

Fig. 1. Physical configuration and coordinate system.

Energy Equation:

$$\frac{\partial T}{\partial t}+u\frac{\partial T}{\partial x}+v\frac{\partial T}{\partial y}=\frac{\kappa}{\rho c_p}\frac{\partial^2 T}{\partial y^2}+\frac{\upsilon}{c_p}\left(\frac{\partial u}{\partial y}\right)^2-\frac{1}{\rho c_p}\frac{\partial q_r}{\partial y}-\frac{Q_0}{\rho c_p}(T-T_\infty)+\frac{Q_1^*}{\rho c_p}(C-C_\infty)+\frac{\sigma' B_0^2 u^2}{\rho c_p}+\frac{D_m \kappa_T}{c_s c_p}\frac{\partial^2 C}{\partial y^2} \tag{3}$$

Concentration Equation:

$$\frac{\partial C}{\partial t}+u\frac{\partial C}{\partial x}+v\frac{\partial C}{\partial y}=D_m\left(\frac{\partial^2 C}{\partial y^2}\right)+\frac{D_m \kappa_T}{c_s c_p}\frac{\partial^2 T}{\partial y^2}-K_c(C-C_\infty)^p \tag{4}$$

With boundary condition,

$$u = U_0\cos(\gamma t),\ T = T_w,\ C = C_w \text{ at } y = 0$$
$$u = 0,\ T = T_\infty,\ C = C_\infty \text{ at } y \to \infty$$

Where, u and v are the velocity component, B_0 is the magnetic field component, β is thermal expansion coefficient, β^* is concentration expansion coefficient, T_w denotes the wall temperature, C_w is the species concentration at the wall, υ is the kinematic viscosity, ρ is density, κ is thermal conductivity, c_p is specific heat at constant pressure, Q_0 denotes the heat sink, Q_1^* denotes the radiation absorption, q_r unidirectional radiative heat flux, K_c for chemical reaction, D_m is coefficient of mass diffusivity, γ denotes oscillating frequency, m is mass per unit area. The radiative heat flux term by using the Rosseland approximation [51] is given by

$$q_r = -\frac{4\sigma_s}{3k_e}\frac{\partial T^4}{\partial y}.$$

where, σ_s is the Stefan-Boltzmann constant and k_e is the mean absorption coefficient, respectively. If temperature differences within the flow are sufficiently small, then the q_r can be linearized by expanding T^4 into the Taylor series about T_∞, which after neglecting higher order terms takes the form by $T^4 \cong 4T_\infty^3 T - 3T_\infty^4$. Then the Eq. (3) becomes,

$$\frac{\partial T}{\partial t}+u\frac{\partial T}{\partial x}+v\frac{\partial T}{\partial y}=\frac{\kappa}{\rho c_p}\frac{\partial^2 T}{\partial y^2}+\frac{\upsilon}{c_p}\left(\frac{\partial u}{\partial y}\right)^2+\frac{16\sigma_s T_\infty^3}{3k_e\rho c_p}\frac{\partial^2 T}{\partial y^2}-\frac{Q_0}{\rho c_p}(T-T_\infty)+\frac{Q_1^*}{\rho c_p}(C-C_\infty)+\frac{\sigma' B_0^2 u^2}{\rho c_p}+\frac{D_m \kappa_T}{c_s c_p}\frac{\partial^2 C}{\partial y^2} \tag{5}$$

From the governing Eqs. (1)–(5) under the initial conditions and the boundary conditions will be based on the finite difference method it is required to make the equations dimensionless. For the purpose introducing the following dimensionless quantities:

$$X=\frac{xU_0}{\upsilon}, Y=\frac{yU_0}{\upsilon}, U=\frac{u}{U_0}, V=\frac{v}{U_0}, \tau=\frac{tU_0^2}{\upsilon}, \theta=\frac{T-T_\infty}{T_w-T_\infty}, \phi=\frac{C-C_\infty}{C_w-C_\infty},$$

So, $x=\frac{X\upsilon}{U_0}, y=\frac{Y\upsilon}{U_0}, u=UU_0, t=\frac{\tau\upsilon}{U_0^2}, T=T_\infty+\theta(T_w-T_\infty)$ and $C=C_\infty+\phi(C_w-C_\infty)$

Dimensionless Governing equations,

$$\frac{\partial U}{\partial X}+\frac{\partial U}{\partial Y}=0 \tag{6}$$

$$\frac{\partial U}{\partial \tau}+U\frac{\partial U}{\partial X}+V\frac{\partial U}{\partial Y}=\frac{\partial^2 U}{\partial Y^2}+G_r\theta+G_c\phi-MU-\frac{1}{D_a}U \tag{7}$$

$$\frac{\partial\theta}{\partial\tau}+\frac{\partial\theta}{\partial Y}U+V\frac{\partial\theta}{\partial Y}=\frac{1}{P_r}\left(1+\frac{16R}{3}\right)\frac{\partial^2\theta}{\partial Y^2}-Q\theta+Q_1\phi + E_c\left(\frac{\partial U}{\partial Y}\right)^2+D_u\frac{\partial^2\phi}{\partial Y^2}+E_cMU^2 \quad (8)$$

$$\frac{\partial\phi}{\partial\tau}+U\frac{\partial\phi}{\partial X}+V\frac{\partial\phi}{\partial Y}=\frac{1}{S_c}\frac{\partial^2\phi}{\partial Y^2}+S_r\frac{\partial^2\theta}{\partial Y^2}-K_r\phi^p \quad (9)$$

Boundary conditions,

$u = U_0\ \cos(\omega\tau),\ T = 1,\ C = 1$ at $y = 0$

$u = 0,\ T = 0,\ C = 0$ at $y \to \infty$

Where, the dimensionless parameters are,

$$\text{Grashofnumber},\ G_r=\frac{g\beta(T_w-T_\infty)\upsilon}{U_0^3},$$

$$\text{massGrashofnumber}.\ G_c=\frac{g\beta^*(C_w-C_\infty)\upsilon}{U_0^3},$$

$$\text{magneticparameter},\ M=\frac{\sigma' B_0^2\upsilon}{\rho U_0^2},$$

$$\text{Darcynumber},\ D_a=\frac{K\prime U_0^2}{\upsilon^2},$$

$$\text{Prandtlnumber},\ P_r=\frac{\rho c_p\upsilon}{\kappa},$$

$$\text{radiationparameter},\ R=\frac{\sigma T_\infty^3}{k_e\kappa},$$

$$\text{heatsinkparameter},\ Q=\frac{Q_0\upsilon}{U_0^2\rho c_p},$$

$$\text{radiationabsorptionparameter},\ Q_1=\frac{Q_1^*\upsilon}{U_0^2\rho c_p},$$

$$\textit{phaseangle}=\omega\tau[\text{Where},\omega=\frac{\gamma\upsilon}{U_0^2}],$$

$$\text{Eckertnumber},\ E_c=\frac{U_0^2}{c_p(T_w-T_\infty)},$$

$$\text{Dufournumber},\ D_u=\frac{D_m\kappa_T}{c_s c_p\upsilon}\left(\frac{C_w-C_\infty}{T_w-T_\infty}\right),$$

$$\text{Soretnumber},\ S_r=\frac{D_m}{\upsilon},$$

$$\text{Schmidtnumber},\ S_c=\frac{\upsilon}{D_m(T_w-T_\infty)},$$

P = Order of chemical reaction and

$$\text{chemicalreaction},\ K_r=\frac{\upsilon K_c(C_w-C_\infty)^{p-1}}{U_0^2}.$$

Stream function ψ satisfies the continuity Eq. (6) and is associated with the velocity components in the usual way as,

$$U=\frac{\partial\psi}{\partial Y}, V=-\frac{\partial\psi}{\partial X}$$

The parameters of technological interest for the present problem are the local skin-friction, the local Nusselt number and the local Sherwood number, which are elucidated as

$$C_f=-\frac{1}{2\sqrt{2}}G_r^{-3/4}\left(\frac{\partial U}{\partial Y}\right)_{Y=0} \quad (10)$$

$$N_u=\frac{1}{\sqrt{2}}G_r^{-3/4}\left(\frac{\partial\theta}{\partial Y}\right)_{Y=0} \quad (11)$$

$$S_h=\frac{1}{2\sqrt{2}}G_r^{-3/4}\left(\frac{\partial\phi}{\partial Y}\right)_{Y=0} \quad (12)$$

3. Numerical solution

To solve the governing second-order coupled non-dimensional partial differential equations with the associated initial and boundary conditions. The method of explicit finite difference has been used to solve (6)–(9) subject to the initial and boundary conditions. For this reason, the area within the boundary layer is divided by some perpendicular lines of *Y*-axis, where the normal of the medium is *Y*- axis as shown in Fig. 2. It is assumed that the maximum length of boundary layer $Y_{\max} = 20$ as corresponds to $Y \to \infty$. i.e.*Y* vary from 0 to 20 and the number of grid spacing in *Y* directions are *m*(=100) and *n*(=200), with the smaller time step $\Delta\tau = 0.005$.

Using the explicit finite difference approximation, we have,

$$\frac{U_{i,j}-U_{i-1,j}}{\Delta X}+\frac{V_{i,j}-V_{i,j-1}}{\Delta Y}=0 \quad (13)$$

$$\frac{U'_{i,j}-U_{i,j}}{\Delta\tau}+U_{i,j}\frac{U_{i,j}-U_{i-1,j}}{\Delta X}+V_{i,j}\frac{U_{i,j+1}-U_{i,j}}{\Delta Y} = \frac{U_{i,j+1}-2U_{i,j}+U_{i,j-1}}{(\Delta Y)^2}+G_r\theta_{i,j}+G_c\phi_{i,j}-\left(M+\frac{1}{D_a}\right)U_{i,j} \quad (14)$$

$$\frac{\theta'_{i,j}-\theta_{i,j}}{\Delta\tau}+U_{i,j}\frac{\theta_{i,j}-\theta_{i-1,j}}{\Delta X}+V_{i,j}\frac{\theta_{i,j+1}-\theta_{i,j}}{\Delta Y} = \frac{1}{P_r}\left(1+\frac{16}{3}R\right)\frac{\theta_{i,j+1}-2\theta_{i,j}+\theta_{i,j-1}}{(\Delta Y)^2}+D_u\frac{\phi_{i,j+1}-2\phi_{i,j}+\phi_{i,j-1}}{(\Delta Y)^2} - Q\theta_{i,j}+Q_1\phi_{i,j}+E_c\left(\frac{U_{i,j+1}-U_{i,j}}{\Delta Y}\right)^2+E_cM(U_{i,j})^2 \quad (15)$$

$$\frac{\phi'_{i,j}-\phi_{i,j}}{\Delta\tau}+U_{i,j}\frac{\phi_{i,j}-\phi_{i-1,j}}{\Delta X}+V_{i,j}\frac{\phi_{i,j+1}-\phi_{i,j}}{\Delta Y} = \frac{1}{S_c}\frac{\phi_{i,j+1}-2\phi_{i,j}+\phi_{i,j-1}}{(\Delta Y)^2}+S_r\frac{\theta_{i,j+1}-2\theta_{i,j}+\theta_{i,j-1}}{(\Delta Y)^2}-K_r(\phi_{i,j})^p \quad (16)$$

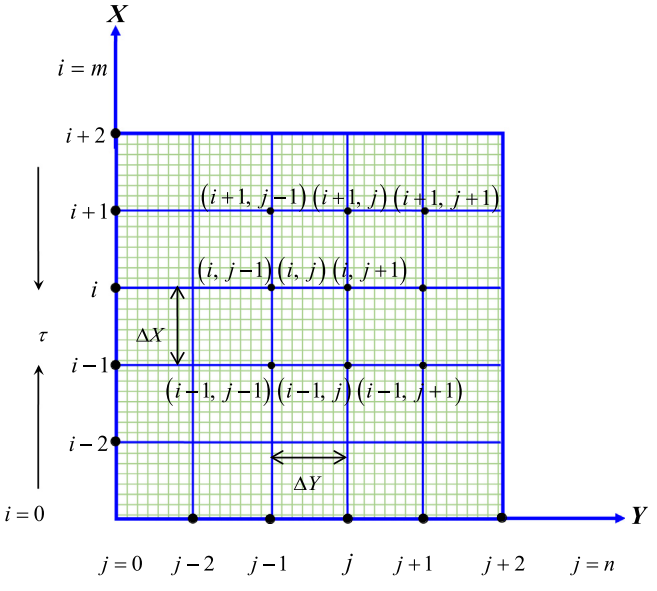

Fig. 2. The finite difference space grid.

The initial and boundary condition with finite difference scheme as

$$U_{i,0}^n = \cos(\omega\tau),\ \theta_{i,0}^n = 1,\ \phi_{i,0}^n = 1$$

$$U_{i,L}^n = 0,\ \theta_{i,L}^n = 0,\ \phi_{i,L}^n = 0 \text{ Where, } L \to \infty$$

where, the subscripts i and j designate the grid points with X and Y coordinates respectively and a value of time, $\tau = n\Delta\tau$, where $n = 1, 2, 3, 4 \ldots\ldots$

4. Stability and convergence analysis of the problem

Here, an explicit finite difference method is being used. The analysis is remained incomplete unless the stability and convergence of the finite difference scheme are discussed. For the constant mesh size, the stability criteria of the scheme may be established as follows. The general terms of the Fourier expansion for U, θ and φ at a time arbitrarily called $t = 0$ are all $e^{i\alpha X}e^{i\beta Y}$ apart from a constant, where $i = \sqrt{-1}$.A time $t = \tau$, these terms becomes,

$$\left.\begin{array}{l} U : \psi_1(\tau)e^{i\alpha X}e^{i\beta Y} \\ \theta : \theta(\tau)e^{i\alpha X}e^{i\beta Y} \\ \varphi : \varphi(\tau)e^{i\alpha X}e^{i\beta Y} \end{array}\right\} \tag{17}$$

After a time step these terms convert to

$$\left.\begin{array}{l} U : \psi_1'(\tau)e^{i\alpha X}e^{i\beta Y} \\ \theta : \theta'(\tau)e^{i\alpha X}e^{i\beta Y} \\ \varphi : \varphi'(\tau)e^{i\alpha X}e^{i\beta Y} \end{array}\right\} \tag{18}$$

Substituting (1) and (2) to the main (13)–(16) equation we get,

$$\psi_1' = \psi_1(\tau) + \Delta\tau\left[G_r\theta + G_c\varphi - \left(M + \frac{1}{D_a}\right)\psi_1 + \frac{2(\cos\beta\Delta Y - 1)}{(\Delta Y)^2}\psi_1 - \frac{U(1 - e^{i\alpha\Delta X})}{\Delta X}\psi_1 - \frac{V(e^{i\beta\Delta Y} - 1)}{\Delta Y}\psi_1\right]$$

$$\Rightarrow \psi_1' = \left[1 + \Delta\tau\frac{2(\cos\beta\Delta Y - 1)}{(\Delta Y)^2} - \Delta\tau\left(M + \frac{1}{D_a}\right) - \frac{U\Delta\tau(1 - e^{i\alpha\Delta X})}{\Delta X} - \frac{V\Delta\tau(e^{i\beta\Delta Y} - 1)}{\Delta Y}\right]\psi_1 + \Delta\tau G_r\theta + \Delta\tau G_c\varphi$$

$$\psi_1' = A_1\psi_1 + A_2\theta + A_3\varphi \tag{19}$$

where, $A_1 = 1 + \Delta\tau\frac{2(\cos\beta\Delta Y - 1)}{(\Delta Y)^2} - \Delta\tau(M + \frac{1}{D_a}) - \frac{U\Delta\tau(1 - e^{i\alpha\Delta X})}{\Delta X} - \frac{V\Delta\tau(e^{i\beta\Delta Y} - 1)}{\Delta Y}$, $A_2 = \Delta\tau G_r$ and $A_3 = \Delta\tau G_c$. For temperature equation,

$$\theta' = \theta + \Delta\tau\left[\frac{1}{P_r}\left(1 + \frac{16R}{3}\right)\frac{2\theta(\cos\beta\Delta Y - 1)}{(\Delta Y)^2} + D_u\frac{2\varphi(\cos\beta\Delta Y - 1)}{(\Delta Y)^2} - Q\theta + Q_1\varphi + E_c\frac{(e^{i\beta\Delta Y} - 1)^2}{\Delta Y^2}\psi_1 - \frac{U(1 - e^{i\alpha\Delta X})}{\Delta X}\psi_1 - \frac{V(e^{i\beta\Delta Y} - 1)}{\Delta Y}\psi_1 + E_cM\psi_1^2\right]$$

$$\theta' = \theta\left[1 + \frac{\Delta\tau}{P_r}\left(1 + \frac{16R}{3}\right)\frac{2(\cos\beta\Delta Y - 1)}{(\Delta Y)^2} - Q\Delta\tau - \frac{U\Delta\tau(1 - e^{i\alpha\Delta X})}{\Delta X} - \frac{V\Delta\tau(e^{i\beta\Delta Y} - 1)}{\Delta Y}\right] + \left[Q_1\Delta\tau + D_u\frac{2\Delta\tau(\cos\beta\Delta Y - 1)}{(\Delta Y)^2}\right]\varphi + E_c\Delta\tau\frac{U(e^{i\beta\Delta Y} - 1)^2}{(\Delta Y)^2}\psi_1 + E_c\Delta\tau M\psi_1^2$$

For obtaining the stability condition, we have to find out Eigen values of the amplification matrix T, but this study is very difficult since all the elements of T are different. Hence, the problem requires that the Eckert number (E_c) is assumed to be very small, that is, tends to zero. Then we get,

$$\theta' = \theta\left[1 + \frac{\Delta\tau}{P_r}\left(1 + \frac{16R}{3}\right)\frac{2(\cos\beta\Delta Y - 1)}{(\Delta Y)^2} - Q\Delta\tau - \frac{U\Delta\tau(1 - e^{i\alpha\Delta X})}{\Delta X} - \frac{V\Delta\tau(e^{i\beta\Delta Y} - 1)}{\Delta Y}\right] + \left[Q_1\Delta\tau + D_u\frac{2\Delta\tau(\cos\beta\Delta Y - 1)}{(\Delta Y)^2}\right]\varphi$$

$$\theta\prime = A_4\theta + A_5\varphi \tag{20}$$

where, $A_4 = 1 + \frac{\Delta\tau}{P_r}(1 + \frac{16R}{3})\frac{2(\cos\beta\Delta Y - 1)}{(\Delta Y)^2} - Q\Delta\tau - \frac{U\Delta\tau(1 - e^{i\alpha\Delta X})}{\Delta X} - \frac{V\Delta\tau(e^{i\beta\Delta Y} - 1)}{\Delta Y}$ and $A_5 = [Q_1\Delta\tau + D_u\frac{2\Delta\tau(\cos\beta\Delta Y - 1)}{(\Delta Y)^2}]$.

For the concentration equation,

$$\varphi\prime = \varphi + \Delta\tau\left[\frac{1}{S_c}\frac{2\varphi(\cos\beta\Delta Y - 1)}{(\Delta Y)^2} + S_r\frac{2(\cos\beta\Delta Y - 1)}{(\Delta Y)^2}\theta - K_r\varphi^P - \frac{U(1 - e^{i\alpha\Delta X})}{\Delta X}\varphi - \frac{V(e^{i\beta\Delta Y} - 1)}{\Delta Y}\varphi\right]$$

$$\varphi\prime = \varphi\left[1 + \frac{2\Delta\tau}{S_c}\frac{(\cos\beta\Delta Y - 1)}{(\Delta Y)^2} - \Delta\tau K_r - \frac{U\Delta\tau(1 - e^{i\alpha\Delta X})}{\Delta X} - \frac{V\Delta\tau(e^{i\beta\Delta Y} - 1)}{\Delta Y}\right] + 2S_r\Delta\tau\frac{(\cos\beta\Delta Y - 1)}{(\Delta Y)^2}\theta$$

$$\varphi\prime = A_6\varphi + A_7\theta \tag{21}$$

where, $A_6 = 1 + \frac{2\Delta\tau}{S_c}\frac{(\cos\beta\Delta Y - 1)}{(\Delta Y)^2} - \Delta\tau K_r - \frac{U\Delta\tau(1 - e^{i\alpha\Delta X})}{\Delta X} - \frac{V\Delta\tau(e^{i\beta\Delta Y} - 1)}{\Delta Y}$ and

$$A_7 = 2S_r\Delta\tau\frac{(\cos\beta\Delta Y - 1)}{(\Delta Y)^2}.$$

Eqs. (19)–(21) can be expressed in the Matrix form,

$$\begin{bmatrix} \psi_1\prime \\ \theta\prime \\ \varphi\prime \end{bmatrix} = \begin{bmatrix} A_1 & A_2 & A_3 \\ 0 & A_4 & A_5 \\ 0 & A_7 & A_6 \end{bmatrix}\begin{bmatrix} \psi_1 \\ \theta \\ \varphi \end{bmatrix}$$

i.e. $\eta\prime = T\prime\eta$

For obtaining the stability condition, Eigen values of the amplification matrix $T\prime$ should be finding out. It is a forth order square matrix. For this explicit finite difference solution, the dimensionless time difference $\Delta\tau$ is very small i.e. tends to zero. Under this condition,

$$A_2 \to 0, A_3 \to 0, A_5 \to 0 and A_7 \to 0$$

$$\therefore T' = \begin{bmatrix} A_1 & 0 & 0 \\ 0 & A_4 & 0 \\ 0 & 0 & A_6 \end{bmatrix}$$

After simplification of the matrix T' the Eigen values are follows, the Eigen values of the amplification matrix T' are obtained as $A_1 = \lambda_1, A_4 = \lambda_2$ and $A_6 = \lambda_3$. For stability test, each of the Eigen values must not exceeded unity in modulus. Under this consideration, the stability conditions are as follows

$$|A_1| \leqslant 1, |A_4| \leqslant 1 and |A_6| \leqslant 1$$

Let, $a_1 = \Delta\tau, b_1 = U\frac{\Delta\tau}{\Delta X}, c_1 = |-V|\frac{\Delta\tau}{\Delta X}$ and$d_1 = 2\frac{\Delta\tau}{(\Delta Y)^2}$ then,

The coefficient of a, b and c are all non-negative. So the maximum modulus of A_1, A_4 and A_6 occurs when $\alpha\Delta Y = n\pi$, where n is integer and hence A_1, A_4 and A_6 are real. The values of $|A_1|$, $|A_4|$ and $|A_6|$ are greater when n is odd integer, in which case;

$$A_1 = 1 - 2[d_1 + a_1\left(M + \frac{1}{Da}\right) + b_1 + c_1]$$

$$A_4 = 1 - 2[d_1\frac{1}{P_r}(1 + \frac{16}{3}R) - \frac{a_1}{2}Q + b_1 + c_1]$$

$$A_6 = 1 - 2[d_1\frac{1}{S_c} + b_1 + c_1 + \frac{a_1}{2}K_c]$$

To satisfied allowable values are $A_1 = -1, A_4 = -1$ and $A_6 = -1$. Hence the stability conditions of the methods are,

$$\frac{2\Delta\tau}{(\Delta Y)^2} + U\frac{\Delta\tau}{\Delta X} + V\frac{\Delta\tau}{\Delta Y} + \Delta\tau\left(M + \frac{1}{Da}\right) \leqslant 1, U\frac{\Delta\tau}{\Delta X} + V\frac{\Delta\tau}{\Delta X} + \frac{2}{P_r}\left(1 + \frac{16}{3}R\right)\frac{\Delta\tau}{(\Delta Y)^2} + \frac{\Delta\tau Q}{2} \leqslant 1 \text{and } U\frac{\Delta\tau}{\Delta X} + V\frac{\Delta\tau}{\Delta X} + \frac{2}{S_c}\frac{\Delta\tau}{(\Delta Y)^2} + \frac{\Delta\tau K_r}{2} \leqslant 1$$

With initial boundary condition and for the values of $\Delta\tau = 0.005$, $\Delta X = 0.20$ and $\Delta Y = 0.25$ then the problem will be converged at $P_r \geqslant 0.164$ and $S_c \geqslant 0.16$. These converge solutions are shown graphically in Figs. 3–15.

5. Results and discussion

The numerical values of non-dimensional velocity, temperature and concentration within the boundary layer for different values of

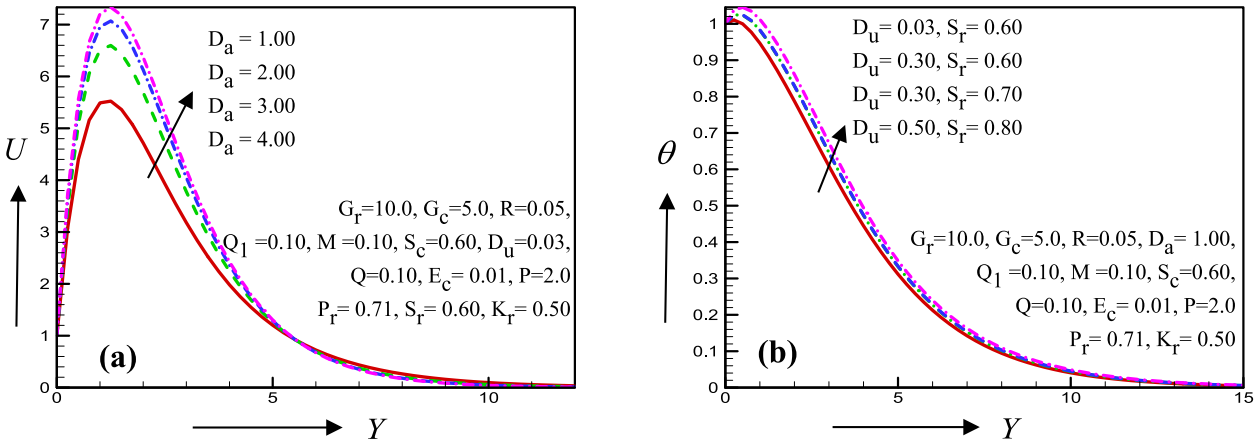

Fig. 3. Illustration of (aw) Velocity profiles for different values of D_a and (b) Temperature for different values of D_u and S_r.

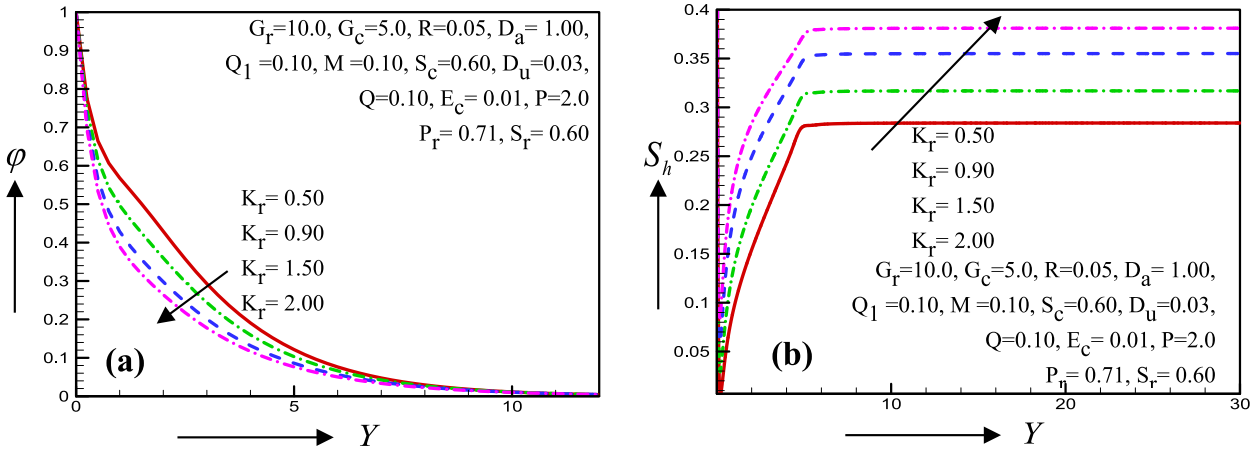

Fig. 4. Illustration of (a) Concentration profiles for different values of K_r and (b) Sherwood number for different values of K_r.

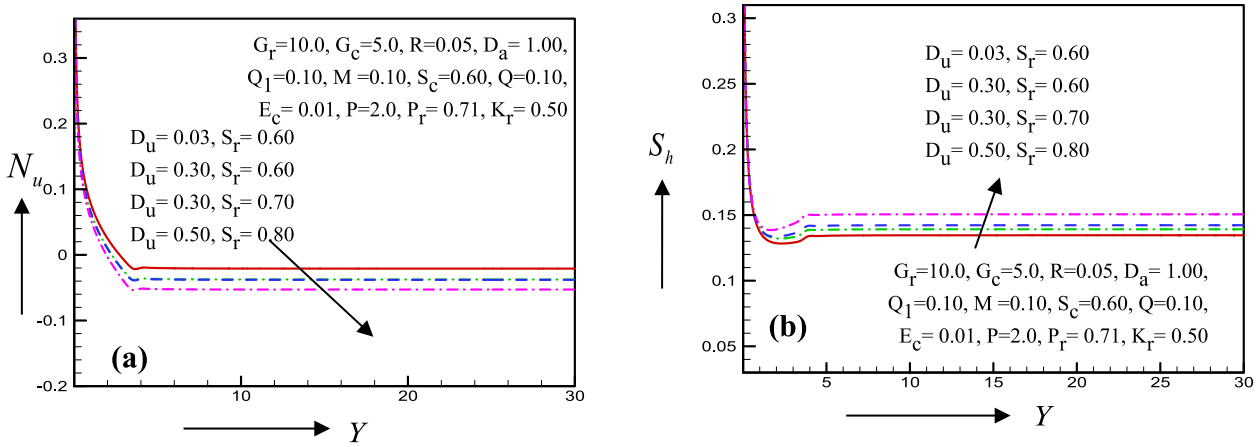

Fig. 5. Illustration of (a) Nusselt number for different Du and S_r and (b) Sherwood number for different values of D_u and S_r.

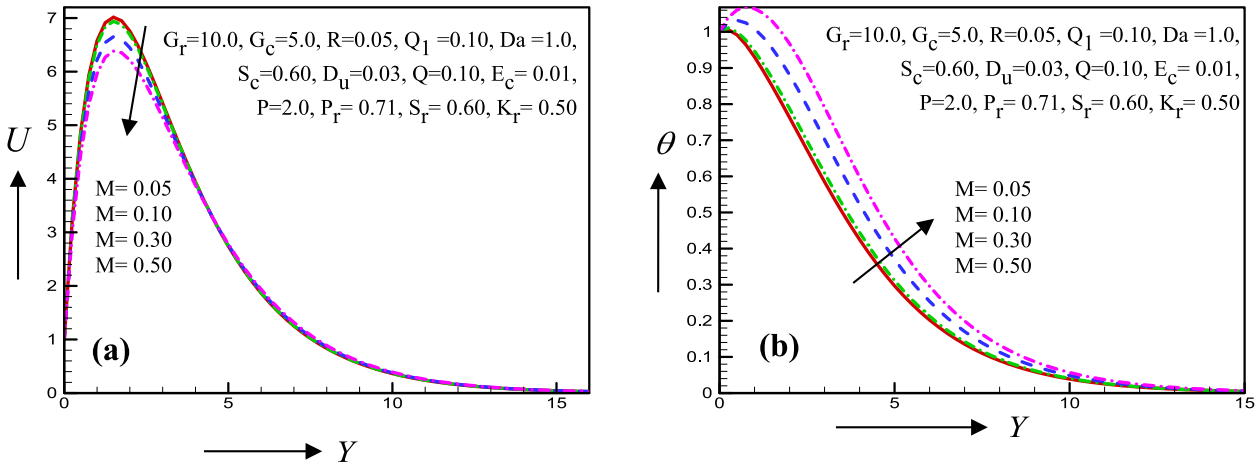

Fig. 6. Illustration of (a) Velocity profiles for different values of M and (b) Temperature profiles for different values of M.

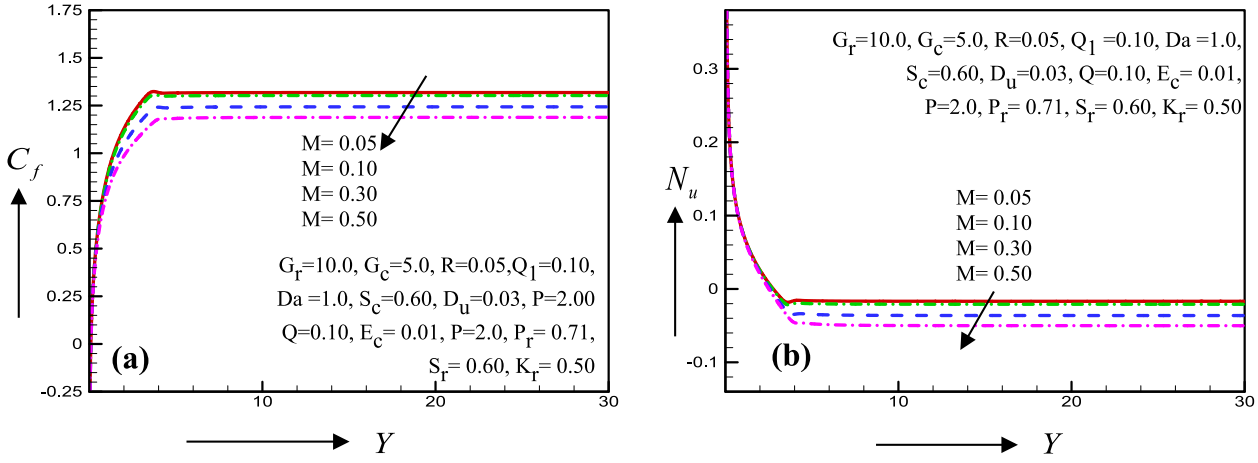

Fig. 7. Illustration of (a) Skin friction for different values of M and (b) Nusselt number for different values of M.

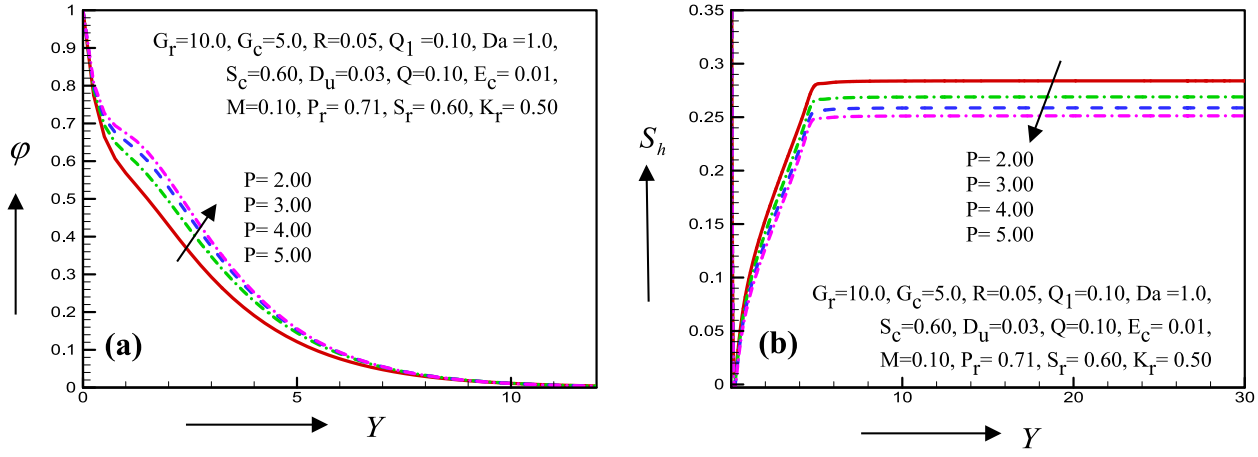

Fig. 8. Illustration of (a) Concentration profiles and (b) Sherwood number for P.

non-dimensional parameter have been computed by a FORTRAN program. For the steady-state solutions, all simulations have been carried out up to dimensionless time, $\tau = 30$. The phase angle parameter, $\omega\tau = 0°$, has been considered, however the effect of this parameter shown in Fig. 13(b).

In Fig. 3(a) the velocity profiles increase in case of strong Darcy number (D_a) and become zero with in short range for same values of Darcy number (D_a). Table 1 provides the numerical value obtained from the EFDM simulation for D_a varies from 1.0 to 4.0. This parameter has a very strong physical significance on the fluid

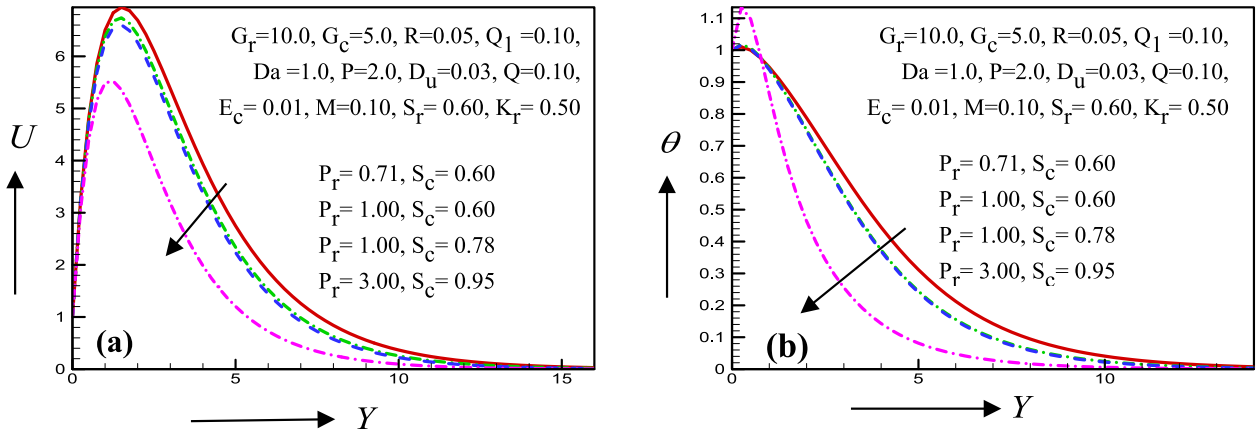

Fig. 9. Illustration of (a) Velocity profiles for different P_r and S_c and (b) Temperature profiles for different P_r and S_c.

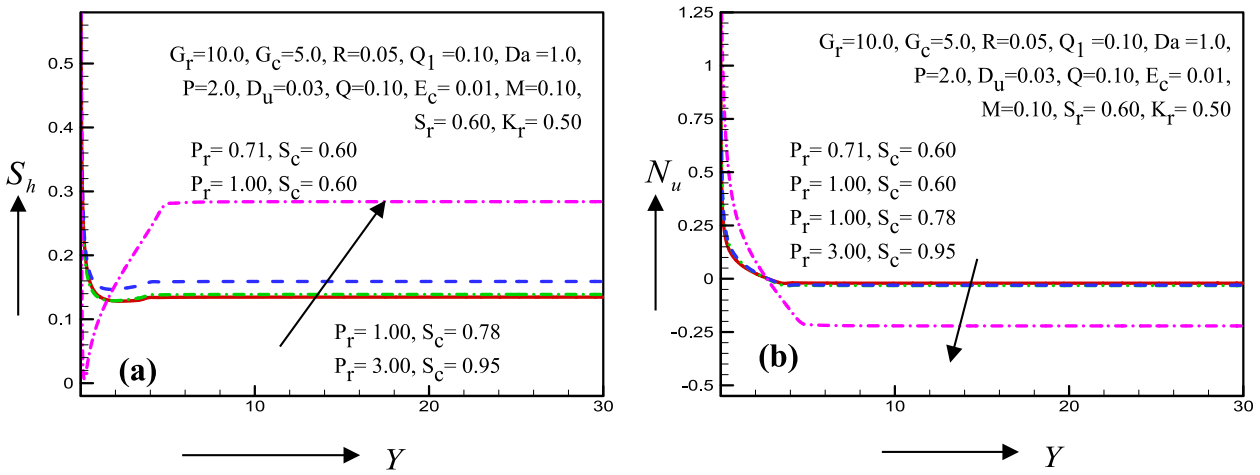

Fig. 10. Illustration of (a) Sherwood number for different values of P_r and S_c and (b) Nusselt number for different P_r and S_c.

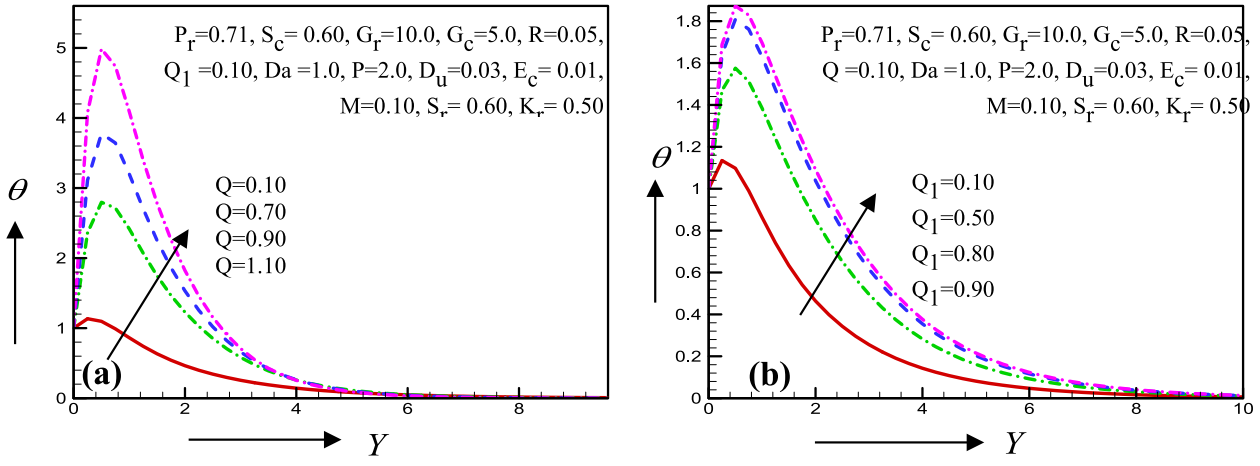

Fig. 11. Illustration of (a) Temperature profiles for different values of Q and (b) Temperature profiles for different values of Q_1.

velocity. It represents the relative consequence of permeability of the porous medium against its cross-sectional area. Porosity is the fraction of the total volume that is taken up by the pore space. To add an additional term in Darcy's Law for inertial effects, permeability associated with that term. The unit's values on it are different, this is because the porous flow always varying with Reynolds number therefore inertial effects are practically non-existent Table 2.

Thermal diffusion (S_r) denotes the quality or state of being homogeneous of mixture composition, the concentration of parts

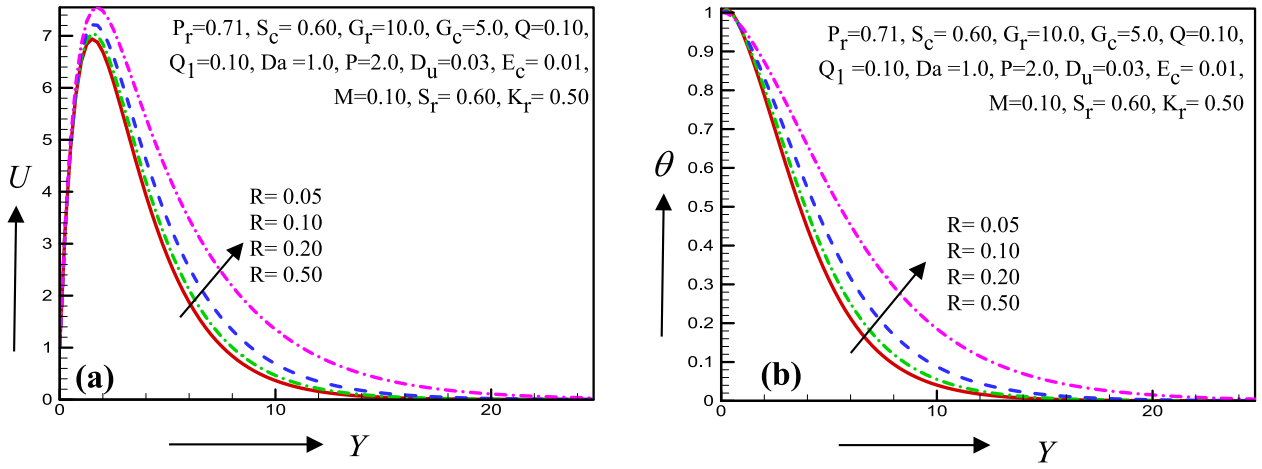

Fig. 12. Illustration of (a) Velocity profiles for different values of R and (b) Temperature profiles for different values of R.

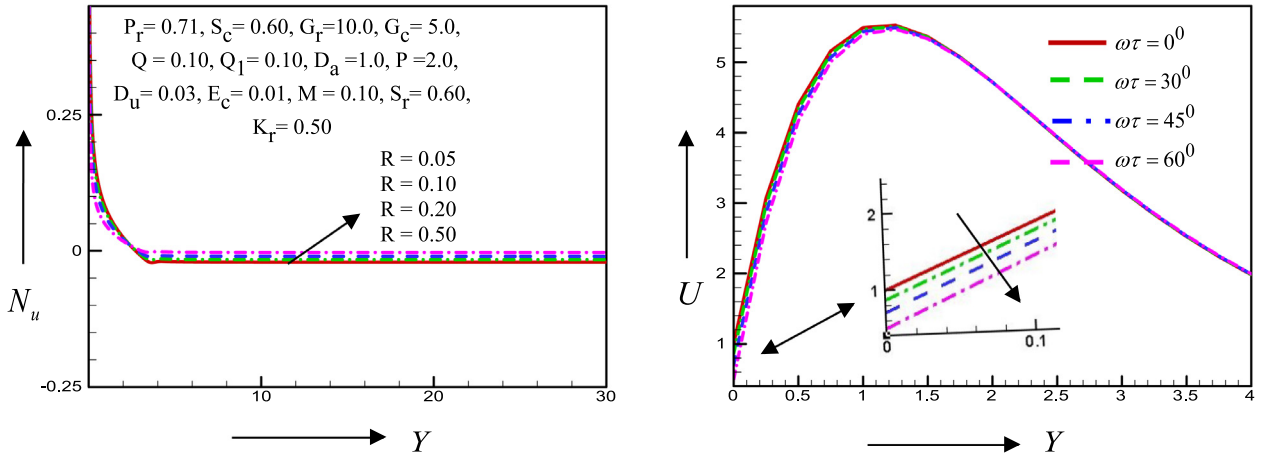

Fig. 13. Illustration of (a) Nusselt number for R and (b) start point of velocity profiles for different values of $\omega\tau$..

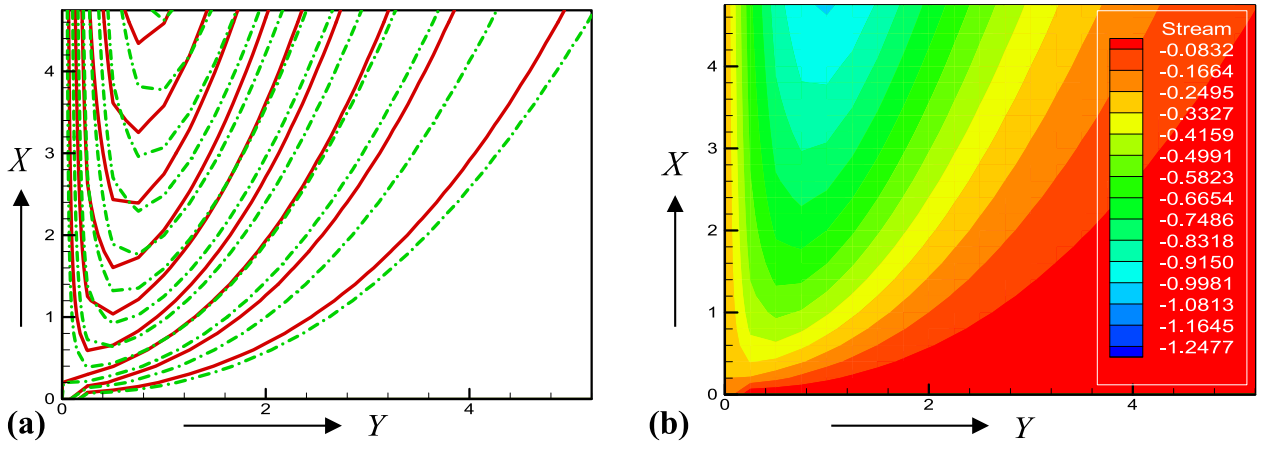

Fig. 14. Illustration of (a) Streamlines R = 0.05 (red solid line) and R = 2.00 (green dashed dot line) for line view and (b) Streamlines flood view.

in the regions of increment and decrement temperatures becomes different. The establishment of a mass gradients cause, in turn, ordinary diffusion, in a non-uniform temperature inhomogeneous state is possible in which the separation effect of thermal diffusion (S_r) is balanced by the counteraction of mass diffusion (D_u). The effects of D_u and S_r on temperature distribution have been shown in Fig. 3(b). Initially the temperature profiles increase on different values of D_u and S_r below the line $X = 1.10$ and after that the

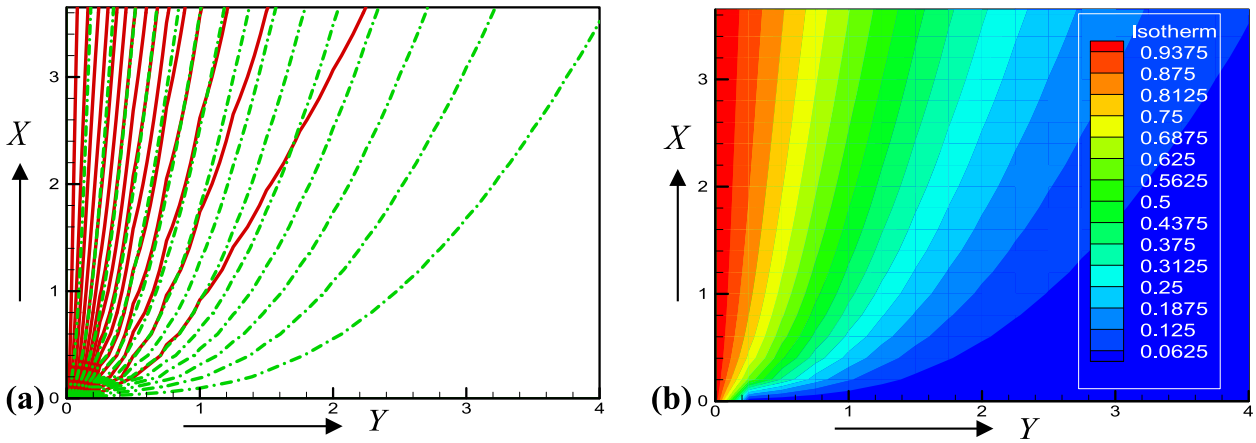

Fig. 15. Illustration of (a) Isotherms R = 0.05 (red solid line) and R = 2.00 (green dashed dot line) for line view and (b) Isotherms flood view.

Table 1
Curve to curve fluctuation for Fig. 3(a) at Y = 1.00.

Velocity profiles		
Value of parameter	Numerical value	Increase/decrease in (%)
D_a = 1.00	5.49026	101.981% increase
D_a = 2.00	6.51007	
D_a = 3.00	6.95590	44.583% increase
D_a = 4.00	7.20445	24.855% increase

temperature begins to decrease with the increase of D_u and S_r. The profiles increase due to mass diffusion (D_u), because mass diffusion (D_u) gradients impact on temperature profiles Table 3.

Fig. 4(a) illustrates that the concentration profiles decrease in case of strong value of chemical reaction parameter (K_r) and become zero with in short range for same values of K_r. Furthermore, the effects of chemical reaction parameter on Sherwood number profiles have been shown in Fig. 4(b). Initially the Sherwood number is observed to be increase on K_r below the line X = 0.4. However, far away from the plate it remains constant with the increase of K_r Table 4.

The different physical phenomena can affect the behaviour of fluid flow such as thermal and mass diffusion. For example, concentration gradients can impact on heat transport and temperature gradients impact on mass transport. In Fig. 5(a), the Nusselt number (N_u) is observed to be decrease in case of different values of D_u and S_r. Similar parameter effect on Sherwood number profiles have

Table 2
Curve to curve fluctuation for Fig. 4(a) at Y = 2.00 and Fig. 4(b) at τ =10.00.

Concentration profiles			Sherwood number profiles		
Value of parameter	Numerical value	Increase/decrease in (%)	Value of parameter	Numerical value	Increase/decrease in (%)
K_r = 0.50	0.42928	97.297% Decrease	K_r = 0.50	0.28380	8.24% increase
K_r = 0.90	0.35978		K_r = 0.90	0.31676	
K_r = 1.50	0.29776	43.51% Decrease	K_r = 1.50	0.35492	6.36% increase
K_r = 2.00	0.26430	24.365% Decrease	K_r = 2.00	0.38088	5.192% increase

Table 3
Curve to curve fluctuation for Fig. 6(a) and (b) at Y = 2.00.

Velocity profiles			Temperature profiles		
Value of parameter	Numerical value	Increase/decrease in (%)	Value of parameter	Numerical value	Increase/decrease in (%)
M = 0.05	6.75607	6.409% Decrease	M = 0.05	0.76270	49.18% increase
M = 0.10	6.69198		M = 0.10	0.78736	
M = 0.30	6.44605	122.965% Decrease	M = 0.30	0.88100	43.18% increase
M = 0.50	6.21583	115.18% Decrease	M = 0.50	0.96736	43.18% increase

Table 4
Curve to curve fluctuation for Fig. 7(a) and (b) at τ =10.0.

Skin friction profiles			Nusselt number profiles		
Value of parameter	Numerical value	Increase/decrease in (%)	Value of parameter	Numerical value	Increase/decrease in (%)
M = 0.05	1.31794	31.02% Decrease	M = 0.05	−0.01676	8.15% Decrease
M = 0.10	1.30243		M = 0.10	−0.02083	
M = 0.30	1.24299	29.72% Decrease	M = 0.30	−0.03608	7.625% Decrease
M = 0.50	1.18746	27.765%Decrease	M = 0.50	−0.04983	6.875% Decrease

also been studied in Fig. 5(b). However, the Sherwood number (S_h) profiles are found to be increase for different parametric values of D_u and S_r Table 5.

The large value of magnetic parameter (M) generates a drag force known as Lorentz force that could be competing against the fluid motion. In Fig. 6(a), the velocity distribution is observed to be decrease due to increase in magnetic parameter (M). However, with the same effect of strong magnetic parameter a reverse phenomenon is occurred in the temperature profiles (Fig. 6(b)) Table 6.

The MHD effects on Skin friction coefficient (C_f) and Nusselt number is exhibited in Fig. 7(a) and (b)respectively. Both Skin friction and Nusselt number profiles is detected to be decrease for the increase of M Table 7.

The effect of order of chemical reaction on the concentration (φ) and Sherwood number (S_h)profiles are illustrated Fig. 8(a) and Fig. 8(b) respectively. The concentration profiles are observed to be rises due to increase of P however an opposite phenomenon is found in the Sherwood number profiles Table 8.

Figs. 9(a)–10(b) represents the effect of Prandtl number (P_r)and Schmidt number (S_c) on velocity, temperature, Sherwood number and The Nusselt number respectively. P_r is the ratio of kinematics viscosity to the thermal diffusivity which is physically very with temperature for example, water $P_r = 7.0$ (At 20 °C), oxygen $P_r = 0.63$ falls more quickly compared to air $P_r = 0.71$. In addition, $S_c$is attributed to the ratio of the momentum diffusivity to the mass diffusivity of the fluid. About the Prandtl number, $P_r << 1$ delineates the thermal diffusivity dominates. For the large values, $P_r >> 1$, the momentum diffusivity dominates the behaviour. For example, the liquid mercury points out that the heat conduction is more consequential compared to convection, so thermal diffusivity influences over others. However, for engine oil, convection is very important in transferring energy from an area in comparison to pure conduction, so momentum diffusivity has the power and influence over others. Fig. 9(a) exhibits that the velocity profiles are decrease for $P_r >> 1$. This behaviour could be attributed to the relative thickness of the hydrodynamic boundary layer and mass transfer boundary layer. Physically, the increase of Schmidt number means a decrease of molecular diffusivity, which corresponds to a decrease of the species boundary layer. It can be seen that, temperature, Sherwood number and Nusselt number profiles decreases due to the increase of Prandtl number (P_r) and Schmidt number (S_c). Due to absorption of heat and radiation, temperature near the plate increase rapidly and after some time it decrease to zero.

Fig. 11(a) exhibits temperature profiles increase rapidly near the plate below $\theta = 5.0$ and far away from the plate it decreases

Table 5
Curve to curve fluctuation for Fig. 8(a) and (b) at Y = 3.00 and τ =3.0.

Concentration profiles			Sherwood number profiles		
Value of parameter	Numerical value	Increase/decrease in (%)	Value of parameter	Numerical value	Increase/decrease in (%)
P = 2.00	0.29286	5.431% increase	P = 2.00	0.19967	1.347% Decrease
P = 3.00	0.34717		P = 3.00	0.18620	
P = 4.00	0.37345	8.059% increase	P = 4.00	0.17675	0.945% Decrease
P = 5.00	0.38784	1.439% increase	P = 5.00	0.16959	0.716% Decrease

Table 6
Curve to curve fluctuation for Fig. 11(a) and (b) at Y = 2.00.

Temperature profiles			Temperature profiles		
Value of parameter	Numerical value	Increase/decrease in (%)	Value of parameter	Numerical value	Increase/decrease in (%)
Q = 0.10	0.46400	127.33% increase	Q_1 = 0.10	0.46400	96.925% increase
Q = 0.70	1.22799		Q_1 = 0.50	0.85170	
Q = 0.90	1.53188	151.945% increase	Q_1 = 0.80	1.03798	62.09% increase
Q = 1.10	1.82237	145.245% increase	Q_1 = 0.90	1.09119	53.21% increase

Table 7
Curve to curve fluctuation for Fig. 12(a) and (b) at Y = 3.00.

Velocity profiles			Temperature profiles		
Value of parameter	Numerical value	Increase/decrease in (%)	Value of parameter	Numerical value	Increase/ decrease in (%)
R = 0.05	5.37875	451.56% increase	R = 0.05	0.60894	65.94% increase
R = 0.10	5.60453		R = 0.10	0.64191	
R = 0.20	5.95384	349.31% increase	R = 0.20	0.68997	48.06% increase
R = 0.50	6.58510	210.42% increase	R = 0.50	0.76861	26.21% increase

Table 8
Curve to curve fluctuation for Fig. 13(b) at Y = 0.00 point that means along the x-axis. Then we can find the starting point of the curves for the oscillating plate phase angle ($\omega\tau$) at 0°, 30°, 45° and 60°.

Velocity profiles starting point of the curves due to phase angle, $\omega\tau$		
Value of Parameter	Starting point numerical values	Increase/Decrease in (%)
$\omega\tau$ = 0°	1.00000	100.0% Decrease
$\omega\tau$ = 30°	0.86600	
$\omega\tau$ = 45°	0.70710	11.236% Decrease
$\omega\tau$ = 60°	0.50000	100.0% Decrease

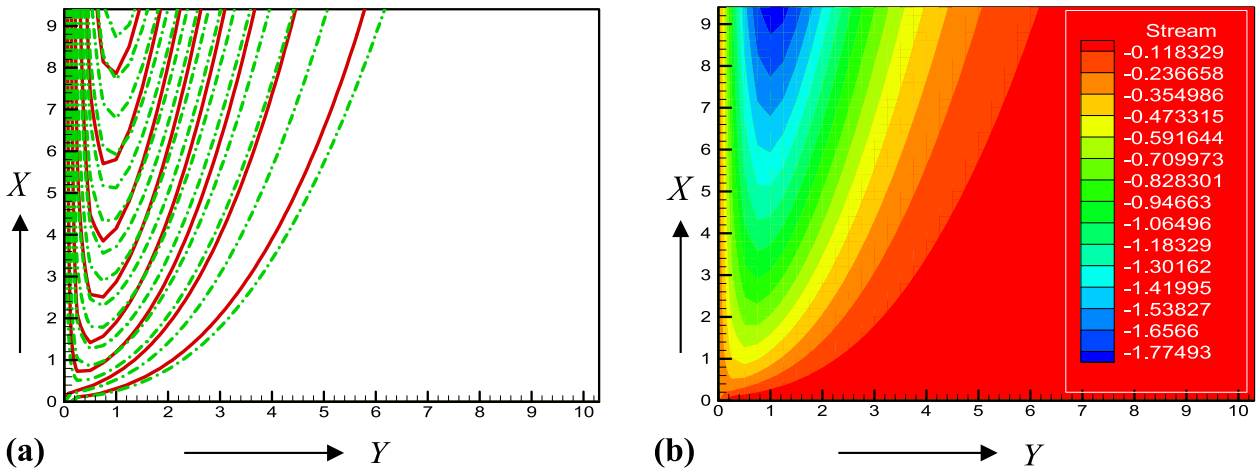

Fig. 16. Illustration of (a) Streamlines $Q_1 = 0.10$ (red solid line) and $Q_1 = 2.00$ (green dashed dot line) for line view and (b) Streamlines flood view.

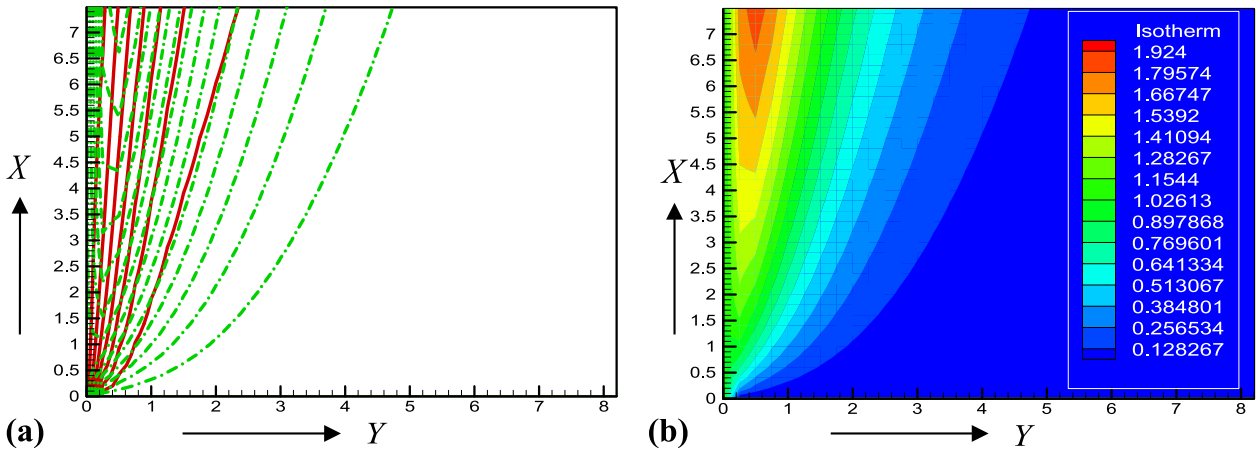

Fig. 17. Illustration of (a) Isotherms $Q_1 = 0.10$ (red solid line) and $Q_1 = 2.00$ (green dashed dot line) for line view and (b) Isotherms flood view.

to zero for the strong heat sink (Q). The effect of radiation absorption parameter, Q_1, on the temperature boundary layer thickness is provided in Fig. 11(b). The temperature profiles show a pick near $\theta = 1.90$ and it decreases to zero away from the plate for increasingQ_1.Therefore, the effect of radiation absorption on the chemically reactive and naturally convective MHD fluid flow is noteworthy. Basically, the molecular fluid particles are being heated by radiation absorption and therefore the particles velocity and buoyancy forces increase. The radiation absorption has some proper characteristics depending on the frequency and wavelengths of the radiation. The transmission of light or of radiant heat is allowed by the propagation of electromagnetic waves in the ether. Electromagnetic waves have similar characteristics to television and radio broadcasting waves they only differ in wavelength. All electromagnetic waves travel at the same speed; therefore, shorter wavelengths are associated with high frequencies. Since fluid is submerged in the ether, due to the vibration of the molecules, fluid can potentially initiate an electromagnetic wave. All bodies generate and receive electromagnetic waves at the expense of its stored energy.

The effects of presence of thermal radiation (R) on the velocity and temperature profiles are shown in Fig. 12(a) and (b). It can be concluded that both profiles increase due to increase in R.

Moreover, the Nusselt number profile is also found increases due to increase in R Fig. 13(a). The effect of the variation of phase angle, $\omega\tau$ (ranges from 0 to 60°) on fluid velocity is shown in Fig. 13(b). The velocity profiles decrease due to increase in $\omega\tau$. In all cases the velocity decays to zero as one move away from the oscillating plate. For larger values of $\omega\tau$ the flow is dominated by inertial effects and the boundary to the flow field is restricted to a shallow layer near the moving plate, the fluid's inertia desires to keep the fluid at rest. For smaller values of $\omega\tau$, viscous effects dominate, and the velocity perturbation caused by the moving plate is felt further inside the large viscosity, the plate can drag more fluid with it. Consequently, the velocity naturally falloffs more slowly as one move away from the plate. For the velocity structure in the oscillating fluid flow boundary layer, Fig. 13(b) is a graph (admittedly somewhat complicated) that shows flow velocity in the laminar oscillatory boundary layer start with different point for the change of phase angle, $\omega\tau$ (ranges for 0–60°). It can be seen that, the phase angle has an effect on the momentum boundary layer thickness and it is significant near the frontier.

For an improved visualization of fluid fields, streamlines can be used. It represents the velocity direction of fluids. The streamlines can be obtained by drawing lines tangent to the flags. They are a rather mathematical object. They can be visualized by implanting

little flags inside the fluid and observing their orientation. The boundary layer system of change can be shown by an isotherm, where the temperature remains constant ($\Delta T = 0$). An isotherm at 0 °C (the freezing point of water) is called the freezing level. This phenomenon occurs when a system is in contact with an outside thermal layer (heat bath), and the change happens gradually enough to allow the system to continually adjust to the temperature of the boundary layer through heat exchange. In this model, we are solving non-dimensional equation after different transformations. For this reason, X and Y-axis have no unit values. It indicates with mash point different. With the stream and isotherms (line view) we can define the difference of boundary layer for different parameters. The legend values of stream and isotherms (flood view) indicate the contours levels. The development of streamlines and isotherms are presented in Figs. 14–17. It can be observed that, momentum boundary layer and thermal boundary layer increases due to the increase of thermal radiation (R). Streamlines and isotherms is presented for the increase of radiation absorption (Q_1) in Figs. 14–17. Furthermore, the momentum and thermal boundary layer are observed to be increases due to the increase of radiation absorption parameter.

6. Conclusions

The Numerical solutions for high speed MHD fluid flow near a moving semi-infinite porous plate with thermal radiation, heat sink, chemical reaction, cross diffusion is analysed, and the following concluding remarks has been observed:

- Velocity profiles increases with the increase in Darcy number, thermal radiation, radiation absorption parameter and combined Prandtl and Schmidt number respectively whilst it decreases due to increase in magnetic parameter. Furthermore, varying of phase angle parameter led the initial point of the velocity curve changes.
- Temperature profile increases due to the increase of magnetic parameter, thermal radiation, cross diffusion, heat sink and radiation absorption respectively whilst it decreases with the increase in the combined Prandtl and Schmidt number.
- Concentration profiles decreases with the increase of chemical reaction parameter whereas it increases with increase in order of chemical reaction parameter.
- Skin friction coefficient profiles was observed to be decrease with increase of magnetic parameter.
- Nusselt number profiles decrease with the increase in magnetic parameter, cross diffusion, and combined Prandtl number and Schmidt number respectively whilst it increases with the increase of thermal radiation parameter.
- Sherwood number profiles increase with the increase of chemical reaction, cross diffusion and combined Prandtl number and Schmidt number respectively whereas it decreases for the increase in the order of chemical reaction.

References

[1] S.Z.A. Zaidi, S.T. Mohyud-Din, Convective heat transfer and MHD effects on two dimensional wall jet flow of a nanofluid with passive control model, Aerosp. Sci. Technol. 49 (2016) 225–230.

[2] X. Ye, J. Zhang, On the behavior of boundary layers of one-dimensional isentropic planar MHD equations with vanishing shear viscosity limit, J. Different. Eq. 260 (2016) 3927–3961.

[3] M. Waqas, M. Farooq, M.I. Khan, A. Alsaedi, T. Hayat, T. Yasmeen, Magnetohydrodynamic (MHD) mixed convection flow of micropolar liquid due to nonlinear stretched sheet with convective condition, Int. J. Heat Mass Transf. 102 (2016) 766–772.

[4] G.S. Seth, B. Kumbhakar, R. Sharma, Unsteady MHD free convection flow with Hall effect of a radiating and heat absorbing fluid past a moving vertical plate with variable ramped temperature, J. Egypt. Mathemat. Soc. 24 (2016) 471–478.

[5] A.M. Rashad, M.A. Ismael, A.J. Chamkha, M.A. Mansour, MHD mixed convection of localized heat source/sink in a nanofluid-filled lid-driven square cavity with partial slip, J. Taiwan Inst. Chem. Eng. 68 (2016) 173–186.

[6] M.S. Khan, I. Karim, M.S. Islam, M. Wahiduzzaman, MHD boundary layer radiative, heat generating and chemical reacting flow past a wedge moving in a nanofluid, Nano Converg. 1 (2014) 20.

[7] O.A. Bég, M.S. Khan, I. Karim, M.M. Alam, M. Ferdows, Explicit numerical study of unsteady hydromagnetic mixed convective nanofluid flow from an exponentially stretching sheet in porous media, Appl. Nanosci. 4 (2014) 943–957.

[8] M. Ferdows, M.S. Khan, O.A. Bég, M.M. Alam, Numerical study of transient magnetohydrodynamic radiative free convection nanofluid flow from a stretching permeable surface, J. Proc. Mech. Eng. (2013) 1–16.

[9] M.S. Khan, I. Karim, L.E. Ali, A. Islam, Unsteady MHD free convection boundary-layer flow of a nanofluid along a stretching sheet with thermal radiation and viscous dissipation effects, Int. Nano Lett. 2 (2012) 24.

[10] M. Ferdows, M.S. Khan, M.M. Alam, S. Sun, MHD Mixed convective boundary layer flow of a nanofluid through a porous medium due to an Exponentially Stretching sheet, Mathemat. Prob. Eng. 3 (2012) 1–21.

[11] I.G. Baoku, B.I. Olajuwon, A.O. Mustapha, Heat and mass transfer on a MHD third grade fluid with partial slip flow past an infinite vertical insulated porous plate in a porous medium, Int. J. Heat Fluid Flow 40 (2013) 81–88.

[12] S. Das, R.N. Jana, O.D. Makinde, Magnetohydrodynamic mixed convective slip flow over an inclined porous plate with viscous dissipation and Joule heating, Alexandria Eng. J. 54 (2015) 251–261.

[13] A. Islam, M.M. Islam, M. Rahman, L.E. Ali, M.S. Khan, Unsteady heat transfer of viscous incompressible boundary layer fluid flow through a porous plate with induced magnetic field, J. Appl. Mathemat. Phys. 4 (2015) 294–306.

[14] M.S. Khan, M. Wahiduzzaman, I. Karim, M.S. Islam, M.M. Alam, Heat generation effects on unsteady mixed convection flow from a vertical porous plate with induced magnetic field, Procedia Eng. 90 (2014) 238–244.

[15] M.V.R. Murthy, R.S. Raju, J.A. Rao, Heat and mass transfer effects on MHD natural convective flow past an infinite vertical porous plate with thermal radiation and hall current, Procedia Eng. 127 (2015) 1330–1337.

[16] V. Ramachandra Prasad, B. Vasu, O.A. Bég, Thermo-diffusion and diffusion-thermo effects on MHD free convection flow past a vertical porous plate embedded in a non-Darcian porous medium, Chem. Eng. J. 173 (2011) 598–606.

[17] V. Ravikumar, M.C. Raju, G.S.S. Raju, Combined effects of heat absorption and MHD on convective Rivlin-Ericksen flow past a semi-infinite vertical porous plate with variable temperature and suction, Ain Shams Eng. J. 5 (2014) 867–875.

[18] R.A. Mohamed, S.M. Abo-Dahab, Influence of chemical reaction and thermal radiation on the heat and mass transfer in MHD micropolar flow over a vertical moving porous plate in a porous medium with heat generation, Int. J. Therm. Sci. 48 (2009) 1800–1813.

[19] S.P.A. Devi, R. Kandasamy, Effects of chemical reaction, heat and mass transfer on non-lenear MHD laminar boundary-layer flow over a wedge with suction or injection, Int. Commun. Heat Mass Transfer 29 (2002) 707–716.

[20] R. Kandasamy, K. Periasamy, K.K. SivagnanaPrabhu, Chemical reaction, heat and mass transfer on MHD flow over a vertical stretching surface with heat source and thermal stratification effects, Int. J. Heat Mass Transf. 48 (2005) 4557–4561.

[21] N.S. Elgazery, The effects of chemical reaction, Hall and ion-slip currents on MHD flow with temperature dependent viscosity and thermal diffusivity, Communications in Nonlinear Science and Numerical Simulation, 14 (2009) 1267–1283.

[22] Y. Zhang, L. Zheng, Analysis of MHD thermosolutal Marangoni convection with the heat generation and a first-order chemical reaction, Chem. Eng. Sci. 69 (2012) 449–455.

[23] M.M. Rahman, M.S. Khan, M.R. Islam, Numerical investigation on MHD fluid flow in the presence of chemical reaction With soret and dufour effects over a vertical plate in a rotating system, J. Appl. Phys. Sci. Int. 4 (2014) 77–88.

[24] F. Mabood, W.A. Khan, A.I.M. Ismail, MHD stagnation point flow and heat transfer impinging on stretching sheet with chemical reaction and transpiration, Chem. Eng. J. 273 (2015) 430–437.

[25] M. Wahiduzzaman, M.S. Khan, I. Karim, MHD convective stagnation flow of nanofluid over a shrinking surface with thermal radiation, heat generation and chemical reaction, Proc. Eng. 105 (2015) 398–405.

[26] M.R. Eid, Chemical reaction effect on MHD boundary-layer flow of two-phase nanofluid model over an exponentially stretching sheet with a heat generation, J. Mol. Liq. 220 (2016) 718–725.

[27] R. Muthuraj, K. Nirmala, S. Srinivas, Influences of chemical reaction and wall properties on MHD Peristaltic transport of a Dusty fluid with Heat and Mass transfer, Alexandria Eng. J. 55 (2016) 597–611.

[28] M.K. Nayak, G.C. Dash, L.P. Singh, Heat and mass transfer effects on MHD viscoelastic fluid over a stretching sheet through porous medium in presence of chemical reaction, Propul. Power Res. 5 (2016) 70–80.

[29] P.B.A. Reddy, Magnetohydrodynamic flow of a Casson fluid over an exponentially inclined permeable stretching surface with thermal radiation and chemical reaction, Ain Shams Eng. J. 7 (2016) 593–602.

[30] S. Srinivas, A. Vijayalakshmi, A. Subramanyam Reddy, T.R. Ramamohan, MHD flow of a nanofluid in an expanding or contracting porous pipe with chemical reaction and heat source/sink, Propul. Power Res. 5 (2016) 134–148.

[31] P.S. Reddy, P. Sreedevi, A.J. Chamkha, MHD boundary layer flow, heat and mass transfer analysis over a rotating disk through porous medium saturated by Cu-water and Ag-water nanofluid with chemical reaction, Powder Technol. 307 (2017) 46–55.
[32] F.S. Ibrahim, A.M. Elaiw, A.A. Bakr, Effect of the chemical reaction and radiation absorption on the unsteady MHD free convection flow past a semi infinite vertical permeable moving plate with heat source and suction, Commun. Nonlinear Sci. Numer. Simul. 13 (2008) 1056–1066.
[33] V. Rubio Hernández, J. Zueco, Network numerical analysis of radiation absorption and chemical effects on unsteady MHD free convection through a porous medium, Int. J. Heat Mass Transf. 64 (2013) 375–383.
[34] P.V. Satya Narayana, B. Venkateswarlu, S. Venkataramana, Effects of Hall current and radiation absorption on MHD micropolar fluid in a rotating system, Ain Shams Eng. J. 4 (2013) 843–854.
[35] V.P. Reddy, R.V.M.S.S.K. Kumar, G.V. Reddy, P.D. Prasad, S.V.K. Varma, Free convection heat and mass transfer flow of chemically reactive and radiation absorption fluid in an aligned magnetic filed, Procedia Eng. 127 (2015) 575–582.
[36] S.M. Arifuzzaman, S.K. Dhali, M.A.K. Azad, B. Roy, Magnetic field and thermal radiation effect on heat and mass transfer of air flow near a moving infinite plate with a constant heat sink, World J. Mechan. 5 (2015) 235–248.
[37] B.M.J. Rana, R. Ahmed, R. Uddin, S.F. Ahmmed, Effect of radiation on unsteady MHD free convective flow past an exponentially accelerated inclined plate, Br. J. Mathemat. Comput. Sci. 19 (2016) 1–13.
[38] P.V. Satya Narayana Effects of variable permeability and radiation absorption on magnetohydrodynamic (MHD) mixed convective flow in a vertical wavy channel with traveling thermal waves Propul. Power Res. 4 2015 150 160
[39] P. Durga Prasad R.V.M.S.S. Kiran Kumar S.V.K. Varma Heat and mass transfer analysis for the MHD flow of nanofluid with radiation absorption Ain Shams Eng. J. 2016.
[40] G. Sreedevi, R. Raghavendra, D.R.V. Rao, A.J. Prasada Rao, Chamkha, Combined influence of radiation absorption and Hall current effects on MHD double-diffusive free convective flow past a stretching sheet, Ain Shams Eng. J. 7 (2016) 383–397.
[41] M. Umamaheswar, M.C. Raju, S.V.K. Varma, J. Gireeshkumar, Numerical investigation of MHD free convection flow of a non-Newtonian fluid past an impulsively started vertical plate in the presence of thermal diffusion and radiation absorption, Alexandria Eng. J. 55 (2016) 2005–2014.
[42] F.M. Hady, R.A. Mohamed, A. Mahdy, MHD free convection flow along a vertical wavy surface with heat generation or absorption effect, Int. Commun. Heat Mass Transfer 33 (2006) 1253–1263.
[43] M.S. Khan, I. Karim, M.H.A. Biswas, Heat generation thermal radiation and chemical reaction effects on MHD mixed convection flow over an unsteady stretching permeable surface, Int. J. Basic Appl. Sci. 1 (2012) 363–377.
[44] M.S. Khan, I. Karim, M.H.A. Biswas, Non-Newtonian MHD mixed convective power-law fluid flow over a vertical stretching sheet with thermal radiation heat generation and chemical reaction effects, Acad. Res. Int. 3 (2012) 80–92.
[45] S.K. Nandy, T.R. Mahapatra, Effects of slip and heat generation/absorption on MHD stagnation flow of nanofluid past a stretching/shrinking surface with convective boundary conditions, Int. J. Heat Mass Transf. 64 (2013) 1091–1100.
[46] L.T. Benos, S.C. Kakarantzas, I.E. Sarris, A.P. Grecos, N.S. Vlachos, Analytical and numerical study of MHD natural convection in a horizontal shallow cavity with heat generation, Int. J. Heat Mass Transf. 75 (2014) 19–30.
[47] B. Ganga, S.M.Y. Ansari, N. Vishnu Ganesh, A.K. Abdul Hakeem, MHD radiative boundary layer flow of nanofluid past a vertical plate with internal heat generation/absorption, viscous and ohmic dissipation effects, J. Nigerian Mathemat. Soc 34 (2015) 181–194.
[48] P.S. Reddy, A.J. Chamkha, Soret and Dufour effects on MHD convective flow of Al_2O_3 – water and TiO_2 – water nanofluids past a stretching sheet in porous media with heat generation/absorption, Adv. Powder Technol. 27 (2016) 1207–1218.
[49] A.H. Srinivasa, A.T. Eswara, Effect of internal heat generation or absorption on MHD free convection from an isothermal truncated cone, Alexandria Eng. J. 55 (2016) 1367–1373.
[50] T. Hayat, T. Muhammad, S.A. Shehzad, A. Alsaedi, An analytical solution for magnetohydrodynamic Oldroyd-B nanofluid flow induced by a stretching sheet with heat generation/absorption, Int. J. Therm. Sci. 111 (2017) 274–288.
[51] C. Perdikis, A. Raptis, Heat transfer of a micropolar fluid by the presence of radiation, Heat Mass Transfer 31 (1996) 381–382.
[52] B. Venkateswarlu, P.V. Satya Narayana, Chemical reaction and radiation absorption effects on the flow and heat transfer of a nanofluid in a rotating system, Appl. Nanosci. 5 (2015) 351–360.
[53] D. Harish Babu, P.V. Satya Narayana, Influence of variable permeability andradiation absorption on heat and mass transfer in MHD micropolar flow over a vertical moving porous plate, ISRN Thermodynamics (2013) 17. Article ID 953536.